Letters in Applied NanoBioScience
Open-Access Journal (ISSN: 2284-6808)

Article
Volume 13, Issue 4, 2024, 171
https://doi.org/10.33263/LIANBS134.171

Utilization of *Parthenium hysterophorus* for the Synthesis of Lignin-ZnO Nanocomposites Aimed at Boosting Antibacterial and Antioxidant Activity

Naveen Kumar [1], Ritu Sharma [1], Neeraj K. Aggarwal [1,*], Akhlash P. Singh [2]

[1] Department of Microbiology, Kurukshetra University, Kurukshetra, 136119, Haryana, India
[2] Department of Biochemistry GGDSD College Chandigarh
* Correspondence: nkumar@kuk.ac.in (N.K.A.);

Scopus Author ID 36875215600
Received: 9.09.2023; Accepted: 7.07.2024; Published: 27.08.2024

Abstract: The dual objective of employing affordable lignin derived from *parthenium* weed biomass is to reduce *Parthenium hysterophorus* weed biomass waste and transform it into valuable substances. In this context, we outline the process of enhancing the value of weed-derived lignin through its direct application in the creation of lignin-ZnO nanocomposites. The present study assesses the efficiency of alkali lignin extracted from *P. hysterophorus* biomass using ultrasonication pretreatment with NaOH assistance. The optimized pretreatment process employing a substrate concentration of 1% (w/v) and a combination of 1.5 NaOH with 30 minutes of sonication led to a reduction in lignin content of 73.55% (w/w) compared to the original biomass. The delignification of lignin was verified through compositional analysis of the treated biomass. The nanomaterials derived from lignin displayed strong promise as antioxidants and antibacterial agents, owing to the collaborative influence of lignin and zinc oxide. This environmentally friendly, economically efficient, one-step synthesis method for creating zinc oxide nanocomposites from lignin not only aids in reducing *P. hysterophorus* waste but also facilitates the generation of value-added materials. This supports the idea that *P. hysterophorus* holds significant promise as an unconventional lignocellulosic source for crafting alkali lignin-ZnO nanocomposites.

Keywords: *P. hysterophorus*; lignin-ZnONCs; antibacterial; antioxidants.

© 2024 by the authors. This article is an open-access article distributed under the terms and conditions of the Creative Commons Attribution (CC BY) license (https://creativecommons.org/licenses/by/4.0/).

1. Introduction

Parthenium hysterophorus, a member of the Asteraceae family, is called Congress grass. This highly invasive annual herbaceous weed is notorious for its robust growth, particularly in warmer climates [1]. Over the last century, it has spread to continents such as Africa, Australia, Asia, and the Pacific Islands, earning its place as one of the world's top seven destructive and dangerous weeds. With an impressive reproductive capacity, a single plant can produce between 10,000 to 15,000 viable seeds, which have the ability to disperse and germinate, rapidly covering extensive areas [2]. This invasive weed is widespread in India, affecting approximately 35 million ha of land [3]. Potential use for *P. hysterophorus* might involve its incorporation into the eco-friendly production of nanoparticles, potentially transforming this troublesome weed into a valuable resource for the emerging nanotechnology sectors.

In recent research developments, scientists have grown interested in the intersection of biology and nanoscience, as evidenced by numerous studies [4]. Over recent years, nanomaterials, especially metal nanocomposites, have garnered significant attention due to their wide-ranging applications spanning fields such as materials science and biotechnology. The preparation of various types of nanoparticles using different weed plants, such as *P. hysterophorus*, has gained significant interest [5]. Nanocomposites are a specific category of composites characterized by an ultrafine phase dimension ranging from 1 to 100 nm [6].

Lignin is a complex polymer found in the cell walls of plants, including *P. hysterophorus* weed. It provides structural support and rigidity to plant tissues. Lignin holds substantial potential for various value-added applications that can greatly impact multiple industries. In recent years, there has been considerable interest in lignin-based materials with impressive UV-absorbent characteristics [7]. ZnO nanomaterials have gained significant popularity due to their outstanding UV protection properties. The lignin-based metal oxide nanocomposites (MONPs) benefit from UV filters that consist of organic and inorganic constituents. Therefore, the lignin-based MONPs exhibit a synergistic impact in providing UV protection, making them one of the most optimal choices among all the existing UV protection agents. Lignin is a highly promising biopolymer that provides UV protection and is used as a replacement for chemical UV absorbers. Lignin has UV-protective properties because of the presence of chromophores. Furthermore, MONPs (ZnO and TiO_2) are frequently included in a wide range of sunscreens due to their widely recognized ability to protect against UV radiation. These results show that mixing lignin with MONPs like zinc oxide and titanium oxide makes the UV protection of the composite materials even better [8]. However, ZnO nanoparticles often encounter aggregation and low dispersibility challenges, primarily due to their hydrophilic and polar nature [9]. Nanoparticles tend to aggregate and eventually settle due to their large surface area and high energy. In addition, smaller particles with a higher diffusion coefficient than larger ones of equal mass rapidly aggregate in the solution due to Brownian motion.

Furthermore, the particles' velocity in the dispersion medium is determined by their particle size, as described by Stoke's Law [10, 11]. To address this issue, incorporating lignin as a dopant in ZnO nanomaterials presents a valuable solution to enhance their dispersibility and reduce aggregation. In recent times, ZnO-NPs have gained considerable recognition for their pivotal role in various biological applications due to their exceptional biocompatibility, cost-effectiveness, and minimal toxicity, as documented by Abid et al. [12]. Moreover, these nanoparticles exhibit a wide range of valuable attributes, including their antibacterial, antifungal, UV-blocking, robust catalytic, and photocatalytic properties, as indicated by studies such as those by Xu et al. [13].

P. hysterophorus is a vigorously spreading herbaceous weed with numerous medicinal attributes, including antioxidant, antibacterial, antitumor, and antitrypanosomal properties. The current investigation sought to create lignin-ZnO nanocomposites (Lignin-ZnONCs) using an alkali lignin extract obtained from *P. hysterophorus* biomass. The resulting nanocomposites underwent UV-vis, FTIR, and SEM analysis, focusing on evaluating their antibacterial and antioxidant potential.

2. Materials and Methods

2.1. Material.

The biomass of *P. hysterophorus* was gathered from the Kurukshetra University campus in Kurukshetra, Haryana, India. They were washed sequentially with distilled water and subsequently air-dried. For subsequent investigation, the dried biomass was finely powdered using a mixer grinder (SUJATA grinder).

2.2. Ultrasound-assisted NaOH pretreatment.

The US-NaOH pretreatment is performed using an SB-120DTN sonicator. To initiate the process, two grams of weed powder were combined with 20 mL of a 1.5% NaOH solution, maintaining a solid-to-liquid ratio of 1:10 (w/v). These mixtures underwent sonication at a temperature of 40°C for 40 minutes, aiming to break down the biomass. Following sonication, the pretreated sample was subjected to autoclaving at 121°C for 30 minutes and stored for future analysis. The solid residues were separated through filtration using a vacuum pump (Rocker 300). Filtrate comes out, which is alkali lignin waste. The alkali lignin extract was filtered [Whatman No. 1 filter paper (0.44 lm)] and centrifuged at 10,000 rpm for 10 minutes; then, the supernatant was used in lignin-ZnO nanocomposite synthesis. The resulting solid portions were dried until they reached a constant weight and then stored at room temperature for compositional analysis.

2.3. Compositional analysis.

2.3.1 Estimation of cellulose.

To determine the cellulose content in 1 gram of oven-dried biomass (whether it was treated or untreated), we subjected it to a mixture of 10 ml of 80% acetic acid and 1.5 ml of nitric acid for 20 minutes. This process resulted in the dissolution of the lignin and hemicellulose components within the biomass [14]. We employed gravimetric analysis to establish the remaining cellulose content in the solid portion [15]. Subsequently, the contents were filtered through pre-weighed filtering crucibles (W_1) with the assistance of a vacuum pump (Rocker 300). These crucibles were then subjected to oven drying at 105°C until they reached a constant weight (W_2). The cellulose content (%w/w) was determined using the following formula:

$$Cellulose\ Content\ (\%) = \frac{W_2 - W_1}{W_0} \times 100 \quad (1)$$

2.3.2 Estimation of hemicellulose.

One gram of desiccated biomass was subjected to a 10 ml solution of 0.5 mol sodium hydroxide (referred to as W_0). This mixture was heated at 80°C for 3.5 hours with continuous stirring. Following this, the contents were filtered through glass crucibles, which had been previously dried, and their weight measured (designated as W_1). The filtrate was rinsed with distilled water until the pH of the rinse liquid reached a neutral level. The solid residue contained in the crucible was then dried in an oven at 105°C until it achieved a constant weight (represented as W_2). To calculate the hemicellulose content (%w/w), we subtracted the weight of the sample before and after this particular treatment, as per reference [16]:

$$Hemiellulose\ Content\ (\%) = \frac{(W_0) - W_2 - W_1}{W_0} \times 100 \quad (2)$$

2.3.3 Estimation of lignin.

The technique outlined by Yao and colleagues [17] was employed to determine the lignin content. In this process, the dried biomass (referred to as W_0) underwent hydrolysis with 72% sulfuric acid at a temperature of 20°C for a duration of 2 h with a bath ratio of 1:15. It's important to note that during this procedure, both cellulose and hemicellulose underwent hydrolysis as well [18]. Subsequently, the contents were filtered through glass crucibles, which had been previously dried and weighed (designated as W_1). The solid residue collected in the crucible was washed with hot water and then dried in an oven at 105°C until a consistent weight was achieved (denoted as W_2). The difference in weight before and after the acid hydrolysis process was utilized to calculate the percentage of lignin content (w/w):

$$Lignin\ Content\ (\%) = \frac{W_2 - W_1}{W_0} \times 100 \quad (3)$$

2.4. Synthesis of lignin-ZnONCs.

Lignin-ZnONCs were synthesized via the method of Prasad Mane et al. with small modifications [19]. A 150-ml beaker was used for the experiment. Initially, 35 ml of a 0.02 M zinc acetate solution was poured into the flask. The weed powder in a 1.5% NaOH solution and supernatant (alkali lignin) was used to synthesize the lignin-ZnO nanocomposites. Subsequently, the alkali lignin extract, 2 ml in volume, was added slowly, drop by drop. The resulting mixture was then subjected to continuous vigorous stirring at room temperature for a duration of 4-5 hours. Next, a 2.0 M sodium hydroxide solution was slowly added while stirring continuously to obtain a slightly yellow solution. The solution was left at room temperature overnight. The resulting white precipitate of Zinc hydroxide settled at the bottom of the conical flask. The Zinc hydroxide precipitate was rinsed with distilled water two to three times, followed by washing with methanol three to four times. After air-drying, it was calcined at 400°C for three hours to obtain Lignin-ZnONCs.

2.5. Characterization of lignin-ZnONCs.

Synthesized alkali lignin-ZnONCs were examined for their cross-sectional morphology and distinctive surface using SEM (SHIMADZU). The sample was broken after freezing in liquid nitrogen. The sample was coated with palladium to obtain resolved micrographs. The image was taken at an accelerated voltage of 10 KV. The initial analysis of the reaction mixture's bio-reduction was performed using UV-visible spectroscopy (SHIMADZU UV-1900 UV-VIS Spectrophotometer). The spectral analysis covered a wavelength range of 250 to 500 nm. To determine the chemical components and potential biomolecules of Lignin-ZnONCs, FTIR (SHIMADZU) was employed. The FTIR spectroscopy of the synthesized Lignin-ZnONCs was recorded within the 300-4000 cm^{-1} range.

2.6. Application of lignin-ZnONCs.

2.6.1. Antibacterial activity.

Gram-negative (*E. coli* MTCC 452) and Gram-positive (*B. subtilis* MTCC 441) bacterial pathogens were procured from the Microbial Type Culture Collection and Gene Bank (MTCC), Chandigarh, India. Nutrient broth was prepared and sterilized in test tubes by

autoclaving at 121°C for 15 minutes. The bacterial strains were individually inoculated into the sterilized nutrient broth and then incubated at 37°C for 24 h. To assess the antibacterial activity of Lignin-ZnONCs, the agar-well diffusion method, described by Seedevi et al. [20], was employed. Nutrient agar plates were used to culture the bacterial strains, and wells were made using a cork borer. Four different concentrations (ranging from 20 to 80 µg/ml) and standard tetracycline (1 mg/ml) were loaded into labeled wells, respectively. The plates were then incubated upright at 37°C for 24 h, after which the zone of inhibition was measured. The diameter of the inhibition zone for each well was recorded and expressed in millimeters.

2.6.2. Antioxidant activity.

The antioxidant potential of the synthesized nanocomposites was evaluated using the DPPH assay. For the experiment, a 0.14 mM DPPH solution was prepared in methanol and kept in the dark at room temperature. Standard solutions of ascorbic acid (ranging from 5 to 30 µg mL^{-1}) and the nanocomposite (50 µg mL^{-1}) were separately prepared in a mixture of ethanol and methanol (1:1). Next, 860 µL of the nanocomposite solution was mixed vigorously with 140 µL of the DPPH radical cation solution. The reaction mixture was then incubated in the dark at 50°C for 30 minutes, and the absorbance was measured at 517 nm [21]. The DPPH solution without the nanocomposites was the negative control, while ascorbic acid was the positive control. These steps were repeated three times to ensure accuracy and reliability.

The percent scavenging by the nanocomposites was calculated with respect to the negative control (DPPH cationic solution without the test sample) (equation (4))

$$\text{Scavenging (\%)} = (Abs_{control} - Abs_{sample})/Abs_{control} \times 100 \quad (4)$$

The term Abs control refers to the absorbance of the DPPH cation radical solution without any nanocomposites, while Abs sample represents the absorbance of the DPPH cation radical solution after it reacts with the nanocomposites. Ascorbic acid (AA) [final concentration 0.25 to 1.5 µg mL^{-1} (10 mL AA + 100 mL ABTS solution + 90 mL deionized water)] was used to make a standard calibration curve for the scavenging capacity. It was also used as a positive control.

3. Results and Discussion

3.1. US-NaOH pretreatment.

Figure 1 illustrates alterations in the biomass makeup of *P. hysterophorus* as the duration of ultrasound-assisted pretreatment with 1.5% NaOH increases, including 20 minutes, 30 minutes, and 40 minutes of sonication. The results presented in Figure 1 indicate that a 30-minute sonication period was effective in achieving the highest level of delignification while preserving the greatest quantity of cellulose in the pretreated biomass. After treatment using 30-minute sonication + 1.5% NaOH, the biomass had 62.28% cellulose (57.83% increase compared to control), 19.52% hemicellulose (37.23% decrease compared to control), and 6.15% lignin (73.55% decrease compared to control) (Figure 1, Table 1). The use of ultrasound-assisted alkaline treatment was favored as a pre-processing method due to its ability to selectively eliminate lignin and hemicellulose without losing cellulose [22].

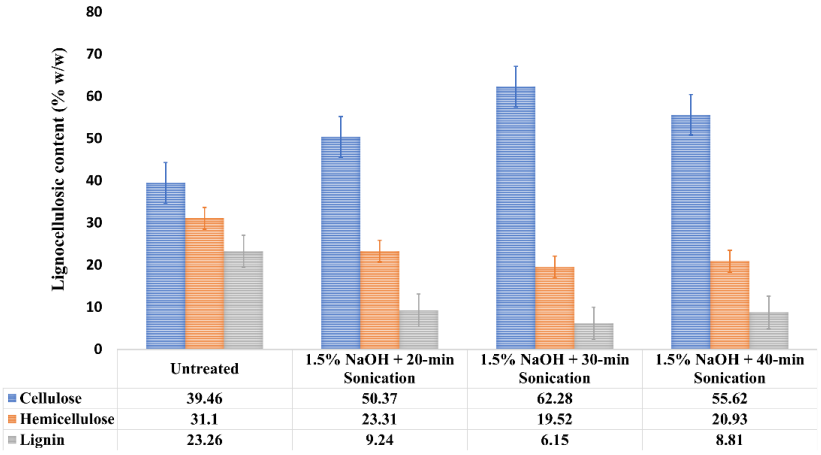

Figure 1. Effect of US-NaOH on *P. hysterophorus* biomass.

Table 1. Effect of US-NaOH pretreatment on biomass composition of *P. hysterophorus*.

NaOH + Sonication	% Change in Biomass Composition		
	Cellulose (%w/w)	Hemicellulose (%w/w)	Lignin (%w/w)
1.5 NaOH + 20-min Sonication	27.64↑	25.04↓	60.27↓
1.5 NaOH + 30-min Sonication	57.83↑	37.23↓	73.55↓
1.5 NaOH + 40 min Sonication	40.95↑	32.70↓	62.12↓

[1] Arrows ↑ and ↓ indicate % increase and % decrease, respectively, in the lignocellulosic content due to the pretreatment, compared to the untreated biomass. Untreated biomass contained 39.46% (w/w) cellulose, 31.1% (w/w) hemicellulose, and 23.26% (w/w) lignin.

3.2. Synthesis of nanocomposite using lignin extract.

Lignin-ZnO nanocomposites were synthesized using alkali lignin obtained from *P. hysterophorus* biomass. The effectiveness of the *P. hysterophorus* biomass-derived lignin in producing lignin-based ZnO nanocomposites was evaluated. Lignin primarily consists of three monolignols: p-coumaryl, coniferyl, and sinapyl alcohols. These monolignols undergo end-wise radical coupling reactions, forming aryl ether and carbon-carbon (C-C) bonds that constitute the lignin polymer [23]. Alkali lignin is extracted from *P. hysterophorus* using ultrasound-assisted alkaline pretreatment, which facilitates the cleavage of β-O-4 bonds and the concurrent formation of aryl glycerol and phenyl glycerol structures. Initially, the optimization process involved adjusting several reaction parameters, including the amounts of zinc acetate and sodium hydroxide, the capping or stabilizing agent concentration, pH level, temperature, choice of mixing method (such as stirring or ultrasonication), drying temperature, and reaction time. These adjustments aimed to achieve the synthesis of Lignin-ZnONCs with optimal properties. Figure 2 illustrates the schematic diagram of the synthesis process for lignin-derived ZnO nanocomposites. The Lignin-ZnONCs were directly synthesized in a one-step process, utilizing lignin derived from *P. hysterophorus* biomass as a capping and stabilizing agent. The reaction mixture initially exhibited a color change from brown to a light-yellow shade, indicating the formation of lignin-capped ZnO nanocomposites (Figure 2). However, the pale-yellow appearance observed in the reaction mixture served as key evidence for the successful formation of lignin-coated ZnO nanocomposites.

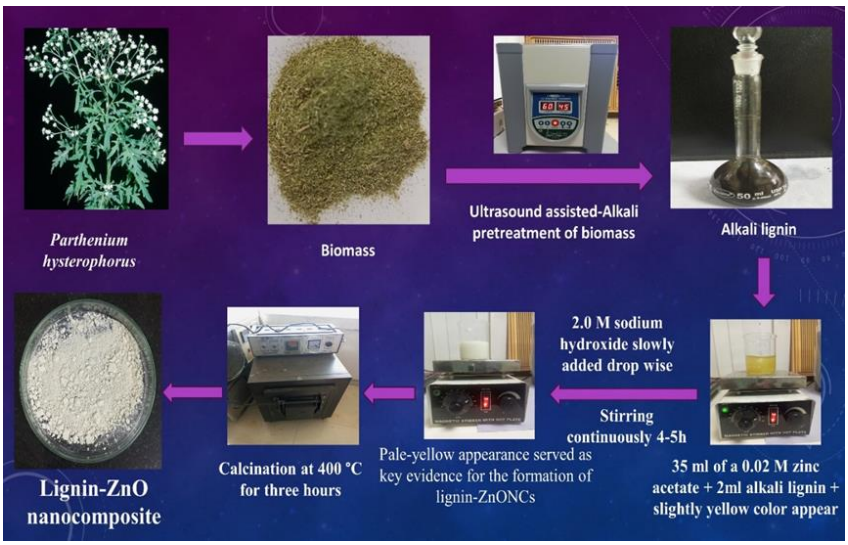

Figure 2. Illustrates the step-by-step process of creating the Lignin-ZnONCs through a synthetic procedure.

3.3. Characterization of lignin-ZnONCs.

Additionally, the UV-visible spectra of these solutions displayed absorption peaks at approximately 270 and 330 nm (Figure 3a), further confirming the presence of both lignin and ZnO in the respective nanocomposites [24]. The ZnO had a similar absorption profile but with exciton absorption at 330 nm, whereas the Lignin-ZnONCs showed an exciton transition at 270 nm, according to UV-VIS absorption spectroscopy (Figure 3a). When ZnO was exposed to UV light, the electrons produced in ZnO would move to the lignin molecules due to the influence of the unsaturated bonds in lignin, facilitating UV absorption [25]. Moreover, the scanning electron microscopy (SEM) analysis confirmed the morphological symmetry of the Lignin-ZnONCs. The SEM image of alkali Lignin-ZnO nanocomposites is given in Figure 3b. It was observed that synthesized nanocomposites are spherical in shape. The image exhibited a flower-like nanostructure with roughness on the surface. Wang et al. [26] have synthesized industrial lignin-derived ZnO nanocomposites and obtained similar results.

On the contrary, the AL/ZnO composite was synthesized using unmodified alkali lignin. Although the addition of AL to the precursor solution significantly influenced the crystal morphology of ZnO, the lignin did not integrate with ZnO to create the lignin-ZnO nanocomposite. The crucial factor for this integration was the incorporation of positively charged quaternary ammonium groups into the AL. During the formation process of the QAL/ZnO nanocomposite, the positively charged groups in QAL were able to attract hydroxyl ions (OH^-), while the negatively charged groups in QAL could attract zinc ions (Zn^{2+}), facilitating the formation of QAL/ZnO hybrid nanocomposites [26]. The synthesized lignin-ZnO nanocomposites were analyzed using FT-IR spectroscopy to identify the distinctive functional groups associated with them.

Additionally, FTIR analysis was conducted to verify the presence of functional groups on the surface of the Lignin-ZnONCs (Figure 3c). The observed peaks reveal the specific functional groups present in the produced lignin-ZnO nanocomposites. The ZnONCs exhibited a distinct band at approximately 422 cm^{-1}, validating the existence of ZnO in the nanocomposites. A broad range of frequencies between 1158 and 1040 cm^{-1} showed that aromatic systems were present in the lignin and the nanocomposites. The lignin-ZnONCs also showed a band centered between 1580 and 1590 cm^{-1}, a typical property of lignin. The presence of hydroxyl groups in lignin resulted in a wide band that was visible in the lignin-ZnONCs

between 3000 and 3600 cm^{-1}. Also, the peak of ZnO NPs is observed in the region of about 500 cm^{-1} [27]. A fragile band around 1,500 cm^{-1} is the characteristic band of the lignin [28]. Following the precursor's annealing process, distinct peaks emerged at 464, 478, and 505 cm^{-1}, indicating Zn-O's transverse optical stretching vibrations. This confirms the existence of zinc oxide nanoparticles [29].

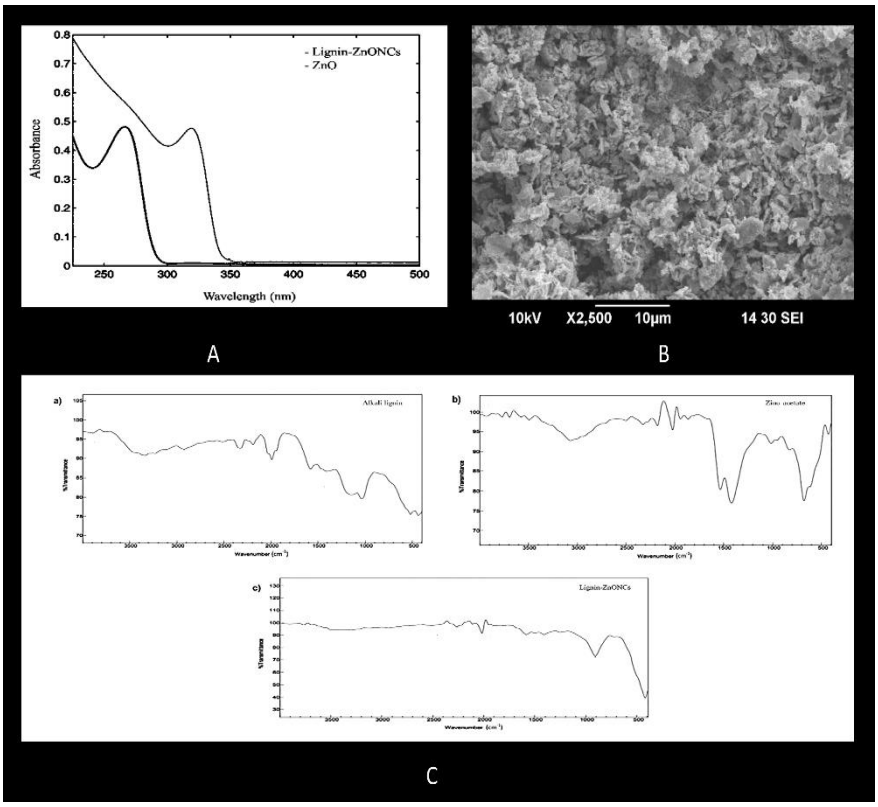

Figure 3. (a) UV-Vis absorption spectra of ZnO and Lignin-ZnONCS; **(b)** SEM image of Lignin-ZnONCs; **(c)** FTIR spectra of lignin, zinc acetate, and Lignin-ZnONCs.

3.4. Application of nanocomposite.

3.4.1. Antibacterial activity of lignin-ZnONCs.

Antibacterial activity refers to the ability of a substance or agent to inhibit the growth and reproduction of bacteria or even kill them outright. It is an essential property in the fields of medicine, healthcare, and various industries where controlling bacterial infections is crucial. Evaluating antibacterial activity typically involves testing the substance or agent against different bacterial strains. The most common method is the agar well diffusion assay, where a sample is applied to a solid agar medium containing bacterial cultures. If the substance possesses antibacterial properties, it will create a clear zone of inhibition around the sample where bacteria growth is inhibited. The size of this inhibition zone indicates the potency of the antibacterial effect. The Lignin-ZnONCs exhibited potent antibacterial properties, demonstrating the highest activity level at a concentration of 80µg/ml (Table 2 and Figure 4). Against *E. coli*, the Lignin-ZnONCs displayed a remarkable 18-mm inhibition zone at this concentration.

Additionally, at 60µg/ml, they showed an impressive 16 mm inhibition zone against *B. subtilis*. The study conducted on Lignin-ZnONCs derived from *P. hysterophorus* revealed their effectiveness against both tested bacterial strains. Both *E. coli* and *B. subtilis* bacterium displayed higher susceptibilities. These findings prove that the alkali lignin extracted from P.

hysterophorus, combined with ZnONCs, is a promising and potent antibacterial agent. Certainly, the results obtained from the zone of inhibition against *E. coli* and *B. subtilis* in this study were found to be superior to those of Ti, Cu, Sn, Ag, and Mg-doped ZnO, as well as Ba-doped CuO and CdO nanostructures (as shown in Table 3).

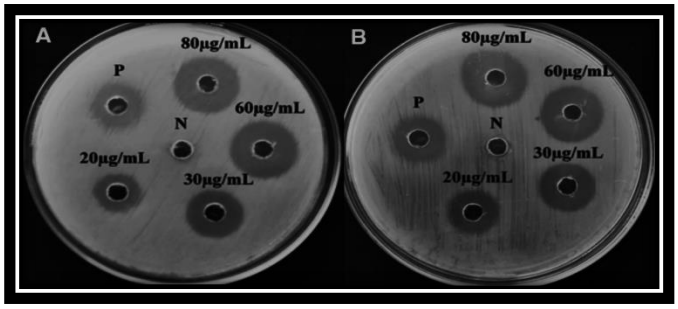

Figure 4. Antibacterial activity Lignin-ZnONCs against pathogens **(A)** *E. coli*; **(B)** *B. subtilis.*

Table 2. Antibacterial activity of Lignin-ZnONCs against pathogens.

	Test Microorganisms		
		E. coli	*B. subtillis*
*Diameter of the inhibition zone (mm)	20 µg/ml	12 ± 0.16	13 ± 0.11
	30 µg/ml	14 ± 0.44	14 ± 0.28
	60 µg/ml	15 ± 0.11	16 ± 0.16
	80 µg/ml	18 ± 0.28	18 ± 0.28
	Positive control (tetracycline)	14 ± 0.26	14 ± 0.26
	Negative control (DMSO)	0	0

*Antimicrobial activity was followed by agar well diffusion method, 0= No zone of inhibition.

Table 3. The inhibition zone diameters against *E. coli* and *B. subtilis* bacteria are compared, as recorded for Lignin-ZnONCs.

Materials	**Synthesis Method**	**Bacteria**	**Zone of Inhibition**	**References**
Ti-doped ZnO nanorods	Wet Chemical Method	*S. aureus* *E. coli*	12 13	[30]
Mg-doped ZnO nanorods	Co-Precipitation Method	*S. aureus* *E. coli*	4 3.5	[31]
Ba-doped CuO nanoparticles	Co-Precipitation Method	*S. aureus* *E. coli*	12 11	[32]
Ba-doped CdO	Chemical Precipitation Method	*S. aureus* *E. coli*	5 6	[33]
nanoparticles	Mechanochemical Processing Technique	*S. aureus* *E. coli*	17 22	[34]
Lignin-ZnONCs	Ultra-sonicated Precipitation Process	*B. subtillis* *E. coli*	18 ± 0.28 18 ± 0.28	Present study

3.4.2. Antioxidant activity of lignin-ZnONCs.

The presence of numerous phenolic groups on a molecule plays a crucial role in determining its antioxidant properties [21]. The results clearly demonstrated that the newly synthesized nanocomposites exhibit significant antioxidant potential, which can be attributed to the combined effect of lignin and ZnO. Interestingly, it was observed that the Lignin-ZnONCs displayed a scavenging effect of 48.39%, while Alkali lignin and Pure ZnO exhibited scavenging effects of 29.13% and 2.38%, respectively (Table 4). Overall, the Lignin-ZnONCs demonstrated the highest efficacy as antioxidants, surpassing even the performance of alkali lignin (29.13%).

Table 4. Determination of the antioxidant potential of Lignin-ZnONCs: DPPH assay.

Types of nanocomposites	**Scavenging effect (%)**
Alkali lignin	29.13±01
Pure ZnO	2.38±06
Lignin-ZnONCs	48.39±06

4. Conclusions

In brief, we have effectively harnessed lignin derived from *P. hysterophorus* biomass using an economical, environmentally friendly synthesis method. Alkali lignin derived from *P. hysterophorus* biomass was used to synthesize Lignin-ZnO nanocomposites. The scanning electron microscopy (SEM) analysis confirmed the symmetrical morphology of these nanocomposites. Notably, the presence of ZnO in the nanocomposites was validated by a distinct band observed at approximately 422 cm^{-1}. The UV-visible spectra of the solutions further supported the existence of both lignin and ZnO, displaying absorption peaks at around 270 and 330 nm. The synthesized nanocomposites exhibited a spherical shape. In terms of antibacterial properties, the Lignin-ZnONCs displayed remarkable effectiveness. Against *E. coli*, it resulted in a significant 18 ± 0.28 mm inhibition zone at a specific concentration.

Moreover, when tested against *B. subtilis* at a 60 µg/ml concentration, it exhibited an impressive 16 ± 0.16 mm inhibition zone. Furthermore, these newly synthesized nanocomposites demonstrated noteworthy antioxidant potential, likely due to the combined effect of lignin and ZnO. Specifically, they exhibited a scavenging effect of 48.39%.

Funding

This research received no external funding.

Acknowledgments

The authors would like to thank the Department of Microbiology, Kurukshetra University, Kurukshetra, Haryana, India, for providing the lab facility for performing the experimentation.

Conflicts of Interest

The authors declare no conflict of interest.

References

1. Kumar, N.; Saharan, V.; Yadav, A.; Aggarwal, N.K. Ultrasound-assisted alkaline pretreatment of Parthenium hysterophorus for fermentable sugar production using a response surface approach. *Sustain. Chem. Clim. Action* **2023**, *2*, 100027, https://doi.org/10.1016/j.scca.2023.100027.
2. Roy, A.; Kumar, P. A Review on The Pharmacological Properties and Other Aspects of *Parthenium Hysterophorus* (L.). *J. Surv. Fish. Sci.* **2023**, *10*, 2073-2089, https://doi.org/10.17762/sfs.v10i2S.1107.
3. Kumar, N.; Mittal, M.; Yadav, A.; Saini, D.K.; Aggarwal, N.K. Statistical optimization of enzymatic saccharification of sodium hydroxide pretreated parthenium hysterophorus biomass using response surface methodology. *J. Wood Chem. Technol.* **2023**, *43*, 1-12, https://doi.org/10.1080/02773813.2022.2145312.
4. Tian, X.; Chong, Y.; Ge, C. Understanding the Nano–Bio Interactions and the Corresponding Biological Responses. *Front. Chem.* **2020**, *8*, 446, https://doi.org/10.3389/fchem.2020.00446.
5. Datta, A.; Patra, C.; Bharadwaj, H.; Kaur, S.; Dimri, N.; Khajuria, R. Green Synthesis of Zinc Oxide Nanoparticles Using *Parthenium hysterophorus* Leaf Extract and Evaluation of their Antibacterial Properties. *J. Biotechnol. Biomater.* **2017**, *7*, 271-276, https://doi.org/10.4172/2155-952X.1000271.
6. Alam, M.M.; Imran, M.; Abutaleb, A.; Khan, M.E.; Ali, W. 4 - Fabrication approaches of nanocomposites. In Nanocomposites-Advanced Materials for Energy and Environmental Aspects, Khan, M.E., Aslam, J., Verma, C., Eds.; Woodhead Publishing, **2023**; 67-85, https://doi.org/10.1016/B978-0-323-99704-1.00020-5.
7. Kai, D.; Tan, M.J.; Chee, P.L.; Chua, Y.K.; Yap, Y.L.; Loh, X.J. Towards lignin-based functional materials in a sustainable world. *Green Chem.* **2016**, *18*, 1175-1200, https://doi.org/10.1039/C5GC02616D.

8. Kaur, R.; Bhardwaj, S.K.; Chandna, S.; Kim, K.-H.; Bhaumik, J. Lignin-based metal oxide nanocomposites for UV protection applications: A review. *J. Clean. Prod.* **2021**, *317*, 128300, https://doi.org/10.1016/j.jclepro.2021.128300.
9. Qian, Y.; Qiu, X.; Zhu, S. Lignin: a nature-inspired sun blocker for broad-spectrum sunscreens. *Green Chem.* **2015**, *17*, 320-324, https://doi.org/10.1039/C4GC01333F.
10. Chapter 6 - Physics of electrorheological fluids. In Studies in Interface Science, Hao, T., Ed.; Elsevier, **2005**; Volume 22, 235-340. https://doi.org/10.1016/S1383-7303(05)80021-3.
11. Kitahata, H.; Yoshinaga, N.; Nagai, K.H.; Sumino, Y. 3 - Dynamics of Droplets. In Pattern Formations and Oscillatory Phenomena, Kinoshita, S., Ed.; Elsevier: Boston, **2013**; 85-118, https://doi.org/10.1016/B978-0-12-397014-5.00003-1.
12. Abid, S.A.; Taha, A.A.; Ismail, R.A.; Mohsin, M.H. Antibacterial and cytotoxic activities of cerium oxide nanoparticles prepared by laser ablation in liquid. *Environ. Sci. Pollut. Res.* **2020**, *27*, 30479-30489, https://doi.org/10.1007/s11356-020-09332-9.
13. Xu, J.; Huang, Y.; Zhu, S.; Abbes, N.; Jing, X.; Zhang, L. A review of the green synthesis of ZnO nanoparticles using plant extracts and their prospects for application in antibacterial textiles. *J. Eng. Fibers Fabr.* **2021**, *16*, 15589250211046242, https://doi.org/10.1177/15589250211046242.
14. Updegraff, D.M. Semimicro determination of cellulose in biological materials. *Anal. Biochem.* **1969**, *32*, 420-424, https://doi.org/10.1016/S0003-2697(69)80009-6.
15. Ahmed, I.; Zia, M.A.; Iqbal, H.M.N. Bioprocessing of Proximally Analyzed WheatStraw for Enhanced Cellulase Productionthrough Process Optimization with *Trichoderma viride* under SSF. *Int. J. Biol. Life Sci.* **2010**, *2*, 100.
16. Di Blasi, C.; Signorelli, G.; Di Russo, C.; Rea, G. Product Distribution from Pyrolysis of Wood and Agricultural Residues. *Ind. Eng. Chem. Res.* **1999**, *38*, 2216-2224, https://doi.org/10.1021/ie980711u.
17. Yao, S.; Wu, G.; Xing, M.; Zhou, S.; Pu, J. DETERMINATION OF LIGNIN CONTENT IN *ACACIA* SPP USING NEAR-INFRARED REFLECTANCE SPECTROSCOPY. *BioResources* **2010**, *5*, 556-562, https://doi.org/10.15376/biores.5.2.556-562.
18. Bhagia, S.; Nunez, A.; Wyman, C.E.; Kumar, R. Robustness of two-step acid hydrolysis procedure for composition analysis of poplar. *Bioresour. Technol.* **2016**, *216*, 1077-1082, https://doi.org/10.1016/j.biortech.2016.04.138.
19. Mane, P.; Shinde, B.; Mundada, P.; Karale, B.; Burungale, A. Biogenic synthesis of ZnO nanoparticles from *Parthenium histerophorus* extract and its catalytic activity for building bioactive polyhydroquinolines. *Res. Chem. Intermed.* **2021**, *47*, 1743-1758, https://doi.org/10.1007/s11164-020-04365-8.
20. Seedevi, P.; Moovendhan, M.; Vairamani, S.; Shanmugam, A. Structural characterization and biomedical properties of sulfated polysaccharide from the gladius of *Sepioteuthis lessoniana* (Lesson, 1831). *Int. J. Biol. Macromol.* **2016**, *85*, 117-125, https://doi.org/10.1016/j.ijbiomac.2015.12.066.
21. Chandna, S.; Thakur, N.S.; Reddy, Y.N.; Kaur, R.; Bhaumik, J. Engineering Lignin Stabilized Bimetallic Nanocomplexes: Structure, Mechanistic Elucidation, Antioxidant, and Antimicrobial Potential. *ACS Biomater. Sci. Eng.* **2019**, *5*, 3212-3227, https://doi.org/10.1021/acsbiomaterials.9b00233.
22. Zhu, S.; Huang, W.; Huang, W.; Wang, K.; Chen, Q.; Wu, Y. Coproduction of xylose, lignosulfonate and ethanol from wheat straw. *Bioresour. Technol.* **2015**, *185*, 234-239, https://doi.org/10.1016/j.biortech.2015.02.115.
23. Behera, S.; Mohapatra, S.; Behera, B.C.; Thatoi, H. Recent updates on green synthesis of lignin nanoparticle and its potential applications in modern biotechnology. *Crit. Rev. Biotechnol.* **2024**, *44*, 774-794, https://doi.org/10.1080/07388551.2023.2229512.
24. Gutiérrez-Hernández, J.M.; Escalante, A.; Murillo-Vázquez, R.N.; Delgado, E.; González, F.J.; Toríz, G. Use of *Agave tequilana*-lignin and zinc oxide nanoparticles for skin photoprotection. *J. Photochem. Photobiol. B: Biol.* **2016**, *163*, 156-161, https://doi.org/10.1016/j.jphotobiol.2016.08.027.
25. Donaldson, L.A.; Radotic, K. Fluorescence lifetime imaging of lignin autofluorescence in normal and compression wood. *J. Microsc.* **2013**, *251*, 178-187, https://doi.org/10.1111/jmi.12059.
26. Wang, H.; Qiu, X.; Liu, W.; Fu, F.; Yang, D. A Novel Lignin/ZnO Hybrid Nanocomposite with Excellent UV-Absorption Ability and Its Application in Transparent Polyurethane Coating. *Ind. Eng. Chem. Res.* **2017**, *56*, 11133-11141, http://dx.doi.org/10.1021/acs.iecr.7b02425.
27. Eivazzadeh-Keihan, R.; Taheri-Ledari, R.; Khosropour, N.; Dalvand, S.; Maleki, A.; Mousavi-Khoshdel, S.M.; Sohrabi, H. Fe_3O_4/GO@melamine-ZnO nanocomposite: A promising versatile tool for organic

catalysis and electrical capacitance. *Colloids Surf. A: Physicochem. Eng. Asp.* **2020**, *587*, 124335, https://doi.org/10.1016/j.colsurfa.2019.124335.
28. Câmara, A.K.F.I.; Okuro, P.K.; Cunha, R.L.d.; Herrero, A.M.; Ruiz-Capillas, C.; Pollonio, M.A.R. Chia (*Salvia hispanica* L.) mucilage as a new fat substitute in emulsified meat products: Technological, physicochemical, and rheological characterization. *LWT* **2020**, *125*, 109193, https://doi.org/10.1016/j.lwt.2020.109193.
29. Jose, L.M.; Kuriakose, S.; Thomas, S. Fabrication, Characterization and In Vitro Antifungal Property Evaluation of Biocompatible Lignin-Stabilized Zinc Oxide Nanoparticles Against Selected Pathogenic Fungal Strains. *BioNanoScience* **2020**, *10*, 583-596, https://doi.org/10.1007/s12668-020-00748-8.
30. Samuel, J.; Suresh, S.; Shabna, S.; Sherlin Vinita, V.; Joslin Ananth, N.; Shajin Shinu, P.M.; Mariappan, A.; simon, T.; Samson, Y.; Biju, C.S. Characterization and antibacterial activity of Ti doped ZnO nanorods prepared by hydrazine assisted wet chemical route. *Phys. E: Low-Dimens. Syst. Nanostructures* **2022**, *143*, 115374, https://doi.org/10.1016/j.physe.2022.115374.
31. Kasi, G.; Viswanathan, K.; Seo, J. Effect of annealing temperature on the morphology and antibacterial activity of Mg-doped zinc oxide nanorods. *Ceram. Int.* **2019**, *45*, 3230-3238, https://doi.org/10.1016/j.ceramint.2018.10.226.
32. Arunadevi, R.; Kavitha, B.; Rajarajan, M.; Suganthi, A.; Jeyamurugan, A. Investigation of the drastic improvement of photocatalytic degradation of Congo red by monoclinic Cd, Ba-CuO nanoparticles and its antimicrobial activities. *Surfaces Interfaces* **2018**, *10*, 32-44, https://doi.org/10.1016/j.surfin.2017.11.004.
33. Sivakumar, S.; Venkatesan, A.; Soundhirarajan, P.; Khatiwada, C.P. Thermal, structural, functional, optical and magnetic studies of pure and Ba doped CdO nanoparticles. *pectrochim. Acta - A: Mol. Biomol. Spectrosc.* **2015**, *151*, 760-772, https://doi.org/10.1016/j.saa.2015.06.105.
34. Talari, M.K.; Abdul Majeed, A.B.; Tripathi, D.K.; Tripathy, M. Synthesis, Characterization and Antimicrobial Investigation of Mechanochemically Processed Silver Doped ZnO Nanoparticles. *Chem. Pharm. Bull.* **2012**, *60*, 818-824, https://doi.org/10.1248/cpb.c110479.